Computational Mechanics 29 (2002) 298–306 © Springer-Verlag 2002
DOI 10.1007/s00466-002-0342-y

Time-dependent creep fracture using singular boundary elements

C. P. Providakis, S. G. Kourtakis

Abstract This paper presents a procedure for modelling singular crack tip regions of creeping, cracked structural components using singular boundary elements. These special boundary elements correctly simulate the time-dependent singular behaviour of stress and strain fields at the crack tip of creeping materials. The investigated structural components are considered to undergo time-dependent, two-dimensional creep deformation and to be subjected to remote loading conditions. The deformation of the components is assumed to be described by the elastic power law creep model. Examples of various crack problems are investigated to illustrate the efficiency of the proposed singular boundary elements for analysing creep stress and strain distribution problems and for determining some important creep fracture parameters. The effectiveness of the proposed approach is demonstrated and its accuracy is compared with the results obtained by finite element solutions for different creep conditions.

Keywords Singular boundary elements, Crack, Viscoplasticity, Creep fracture, Elastic power law creep model, Time-dependent inelasticity

1 Introduction

In fracture mechanics, a main task is the analysis of the crack tip singular stress and strain fields and evaluation of some important fracture parameters which affect crack propagation. The problem is much more complicated if time-dependent inelastic deformations in creeping cracked structural components is considered. A complete analytical solution for this kind of problems does not exist. In early works of Rice and Riedel (1978, 1979, 1980), an asymptotic analysis was performed to give closed-form expressions for creep stresses and strains near the crack tip of cracked specimens. In their analysis, the elastic strain rates were neglected compared with the creep rates, since at the crack tip and for values of creep exponent greater than one, the latter rates are much larger than the former rates. While this assumption is asymptotically correct at the crack tip, this needs careful investigation since the situation may be different even a small distance away from the crack tip. For this reason, and in order to look at realistic and practical problems, the use of numerical solutions such as the finite element method (FEM) and the boundary element method (BEM) becomes imperative. For a review on the subject one can consult Beskos (1987).

In connection with a boundary element determination of near crack tip stress and strain fields in cracked structural components undergoing two-dimensional inelastic deformation one should mention here the works of Mukherjee and his co-workers for Mode I and II (1981a, 1981b) and Mode III (1981c) cracks. In these papers, a stationary crack is modelled as a very thin ellipse and by using a Green's function approach, the stress redistribution in time near the crack tip is obtained. Later, Cruse and Polsch (1986) and Rußwurm (1992) modeled the fields at crack tips by also using appropriate Green's functions, while Tan and Lee (1983) used Kelvin's fundamental solutions and appropriate boundary conditions to simulate the crack. Leitao et al. (1995) proposed a dual-boundary element methodology to numerically simulate elastoplastic crack growth. A more comprehensive review in BEM solutions of inelastic fracture mechanics problems could be found in the review article of Aliabadi (1997).

In the search for an accurate, yet generalized, computational method for evaluating singular crack tip stress and strain fields, the singular element approach in conjunction with BEM has been properly used in various fracture mechanics applications. Several researchers have contributed to this field: Blandford et al. (1981) was the first who introduced the traction singular quarter-point boundary element approach in combination with a multi-domain formulation to the solution of both symmetrical and non-symmetrical crack problems. Thereafter, this approach has been extensively used in the application of the boundary element method to two- and three-dimensional crack problems. An extension of the quarter-point element technique was used by Hantschel et al. (1990) who made an attempt to model crack tip fields arising in two-dimensional elastoplastic cracked panels by introducing some special singular boundary elements which took into account the HRR singularity field (Hutchnison, 1968; Rice and Rosengren, 1968) near the crack tip.

Fracture analyses which take into account time-dependent inelastic deformation problems arising in creeping cracked structural components are, in the BEM literature,

Received: 27 February 2002 / Accepted: 28 May 2002

C. P. Providakis (✉), S. G. Kourtakis
Department of Applied Sciences,
Technical University of Crete GR-73100
Chania, Greece

The authors are grateful to Professor D.E. Beskos for encouragement and helpful discussions during the course of this work.

almost non-existent. To the authors knowledge only the work of Mukherjee's research team, as it is described above, addresses the problem with the use of the Green's function approach. This Green's function approach, although accurate, is however limited to problems with a single crack modelled as a very thin ellipse. The main difficulty for the solution of this kind of fracture problems for both FEM and FEM methodologies is that, while at zero time the form of the stress singularity near crack tip is the well known elastic singularity $r^{-1/2}$ (where r is the distance from the crack tip – see Fig. 1) for any other time step the order of singularity changes to $r^{-1/(m+1)}$ in relation to the creep exponent m. Thus, it is clear that for this kind of problem the singularity order is variable and for a proper numerical solution of the problem one should be able to change the singularity order in a consistent time-dependent manner.

A fracture parameter which has played a very important role in both elastic and inelastic fracture mechanics is the contour integrals developed in paths around crack tips. For creeping materials an energy rate contour integral $C(t)$ has been defined in Bassani and McClintock (1981) for obtaining plane strain finite element solutions of the power-law creep elevation of crack tip stresses subsequent to an initial elastic response. This specific contour integral appears to be a viable parameter for characterizing creep crack growth under steady-state conditions and can be considered as a time and path-dependent amplitude factor of the asymptotic stress field near a crack tip.

In the present paper, a creep strain traction singular element (CR-STSE) is implemented in the direct boundary element formulation to evaluate the time-dependent inelastic stress and strain singularity field distribution involved in creeping cracked two-dimensional plates. This CR-STSE is produced by using the technique presented in Maiti (1992) to simulate power type singularities around crack tips arising in various fracture problems of linear elasticity. The stress and strain results obtained by the implementation of the CR-STSE in the boundary element formulation are used, subsequently, to determine the time dependence of the energy rate contour integral $C(t)$ and the growth of the creep zone. Numerical examples are presented for different test specimens: shallow edge cracked plate and two typical fracture test specimens. These specimens are single edge notched tension (SENT) and compact tension (CT) specimens. The results obtained by the present BEM methodology are further compared with available finite element solutions in the literature. The creep constitutive model used in the numerical calculations is the power law creep model (Nortan, 1929) but any other creep constitutive model having similar mathematical structure can be easily implemented in the proposed algorithm.

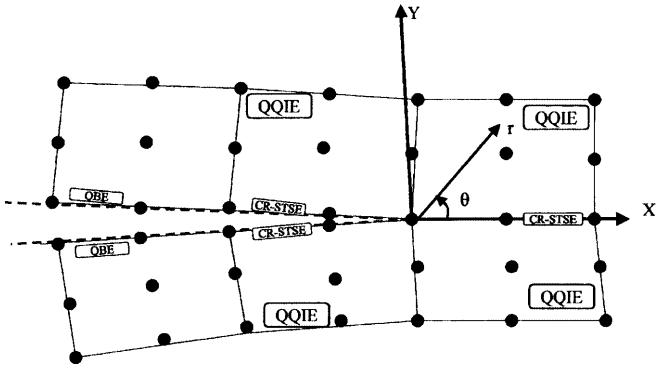

Fig. 1. Geometry of the crack tip

2
Derivation of boundary integral equations

The Navier equation for the displacement rates, in plane strain deformation and under the presence of non-elastic strains can be written as

$$\dot{u}_{i,jj} + \frac{1+\nu}{1-\nu}\dot{u}_{k,ki} = -\frac{\dot{F}_i}{G} + 2\dot{\varepsilon}^n_{ij,j} + \frac{2(1+\nu)}{1-2\nu}(\alpha\dot{T})_{,i} \quad (i,j,k=1,2) \tag{1}$$

where F_i is the prescribed body force per unit volume, G, ν and α are the shear modulus, Poisson's ratio and coefficient of linear thermal expansion, respectively, u_i is the displacement vector. Suitable traction and displacement rate boundary conditions must be prescribed. The integral representation of the solution of a point P on the boundary of the body (with $\dot{F}_i = 0$) has the following initial strain form

$$\begin{aligned}(\delta_{ij} - C_{ij})\dot{u}_i(P) = &\int_\Gamma \left[U_{ij}(P,Q)\dot{\tau}_j(Q) - T_{ij}(P,Q)\dot{u}_j(Q)\right]\mathrm{d}\Gamma_q \\ &+ \int_\Omega [\Sigma_{jki}(P,q)\dot{\varepsilon}^n_{jk}(q) \\ &+ \tilde{\Sigma}_{jki}(P,q)\delta_{jk}\alpha\dot{T}(q)]\mathrm{d}\Omega_q \end{aligned} \tag{2}$$

where δ_{ij} is Kronecker delta, P, Q are boundary points, q is an interior point, Γ and Ω are the boundary and the surface of the body, respectively. The kernels $U_{ij}, T_{ij}, \Sigma_{jki}$ and $\tilde{\Sigma}_{jki}$ are known singular solutions due to a point load in an infinite elastic solid in plane strain (Mukherjee, 1977). The traction and displacement rates are denoted by $\dot{\tau}$ and $\dot{u}$, respectively. The coefficients C_{ij} are known functions of the included angle at the boundary corner at P, the angle between the bisector of the corner angle and the x-axis. Equation (2) is a system of integral equations for the unknown traction and displacements rates in terms of their prescribed values on the boundary, and the non-elastic strain rates. The unknown quantities only appear on the boundary of the body and the surface integrals are known at any time through the constitutive equations.

The stress rates can be obtained by direct differentiation of Eq. (2) resulting in

$$\begin{aligned}\dot{\sigma}_{ij}(p) = &\int_\Gamma \left[\bar{U}_{ijk}(p,Q)\dot{\tau}_k(Q) - \bar{T}_{ijk}(p,Q)\dot{u}_k(Q)\right]\mathrm{d}\Gamma_q \\ &- 2G\dot{\varepsilon}^n_{ij}(p) - 3K\alpha\dot{T}(p)\delta_{ij} \\ &+ \int_\Omega [\bar{\Sigma}_{ijkl}(p,q)\dot{\varepsilon}^n_{kl}(q) + \bar{\tilde{\Sigma}}_{ijkl}(p,q)\delta_{kl}\alpha\dot{T}(q)]\mathrm{d}\Omega_q \end{aligned}$$
$$(i,j,k,l=1,2) \tag{3}$$

where G, K are the shear and bulk modulus, respectively; $\bar{\Sigma}_{ijkl}$ and $\bar{\bar{\Sigma}}_{ijkl}$ are inelastic and temperature effect kernel functions, respectively, which are also defined in the work of Mukherjee (1977).

3 Standard and singular element implementation

Standard boundary and interior surface element implementation

The integral equations (2) and (3) can be expressed in numerical form by discretizing the boundary and the interior into a number of standard three-noded quadratic boundary elements (QBE) (Fig. 2a) and nine-noded quadratic quadrilateral interior surface elements (QQIE) (Fig. 2b), respectively, provided that they are not adjacent to the crack tip. Thus, the discretization of the boundary integrals in Eqs. (2) and (3) is performed by using the coordinates, the displacement and traction rate fields of an arbitrary point within the element Γ_l which can be calculated by the following equations

$$\begin{aligned} \tilde{X}_j &= N_a(\zeta)\tilde{X}_j^a \\ \dot{u}_j &= N_a(\zeta)\dot{U}_j^a \\ \dot{\tau}_j &= N_a(\zeta)\dot{P}_j^a \end{aligned} \tag{4}$$

where $N_a(\zeta)$ is a set of quadratic shape functions of QBE defined on any regular boundary element Γ_l not adjacent to the crack tip and given as

$$\begin{aligned} N_1 &= \zeta(\zeta-1)/2 \\ N_2 &= (1-\zeta^2) \\ N_3 &= \zeta(\zeta+1)/2 \end{aligned} \tag{5}$$

ζ is the intrinsic coordinate on Γ_l which varies between -1 and $+1$ and the subscript α is summed from 1 to 3. $\tilde{X}_j^a$, $\dot{U}_j^a$ and $\dot{P}_j^a$ are vectors containing the nodal values of coordinates, displacement rates and the boundary traction rates, respectively.

The coordinates, the nonelastic strain and the temperature rate fields of an arbitrary interior point ξ within any interior element Ω_i can be calculated by the equations

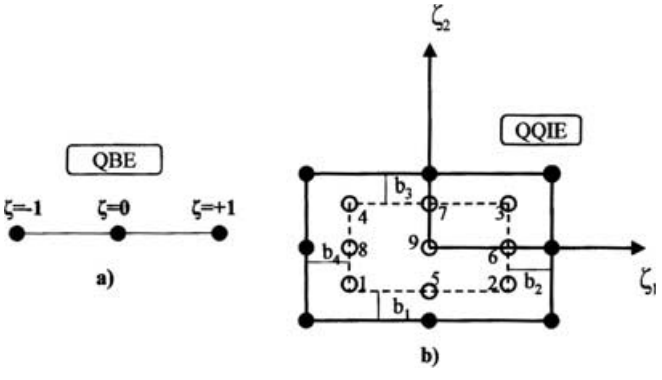

Fig. 2. **a** Quadratic boundary element (QBE), **b** 9-node quadratic quadrilateral interior element (QQIE)

$$\begin{aligned} \tilde{x}_j &= N'_b(\zeta_1,\zeta_2)\tilde{x}_j^b \\ \dot{\varepsilon}_{jk}^n &= N'_b(\zeta_1,\zeta_2)\dot{E}_{jk}^{n^b} \\ \dot{T} &= N'_b(\zeta_1,\zeta_2)\dot{T}^b \end{aligned} \tag{6}$$

where $\tilde{x}_j$ is the vector that contains the Cartesian coordinates of an arbitrary interior point ξ within the element Ω_i and $\tilde{x}_j^b$ is the vector of the Cartesian coordinates related to the nodal point of the element Ω_i; $\dot{E}_{jk}^{n^b}$ and $\dot{T}^b$ represent the vectors of the increments of the nonelastic strain and temperature rates terms at an arbitrary point ξ inside the interior element Ω_i; ζ_1 and ζ_2 are intrinsic coordinates on any interior element Ω_i and the subscript b is summed from 1 to 9; $N'_b(\zeta_1,\zeta_2)$ is a set of polynomial shape functions which, for the purposes of the present paper, is defined for any element Ω_i, by using the standard 9-noded quadratic quadrilateral interpolation shape functions of QQIE defined as

$$\begin{aligned} N'_1 &= \zeta_1\zeta_2\frac{(-\alpha_2+\zeta_1)(-\alpha_3+\zeta_2)}{\alpha_4\alpha_5\alpha_1\alpha_6} \\ N'_2 &= \zeta_1\zeta_2\frac{(-\alpha_4+\zeta_1)(-\alpha_3+\zeta_2)}{\alpha_2\alpha_5\alpha_1\alpha_6} \\ N'_3 &= \zeta_1\zeta_2\frac{(-\alpha_4+\zeta_1)(\alpha_1+\zeta_2)}{\alpha_2\alpha_5\alpha_3\alpha_6} \\ N'_4 &= \zeta_1\zeta_2\frac{(-\alpha_2+\zeta_1)(\alpha_1+\zeta_2)}{\alpha_4\alpha_5\alpha_3\alpha_6} \\ N'_5 &= \zeta_2((\alpha_2-\zeta_1)(\alpha_4+\zeta_1))\frac{(-\alpha_3+\zeta_2)}{\alpha_2\alpha_4\alpha_1\alpha_6} \\ N'_6 &= \zeta_1((\alpha_3-\zeta_2)(\alpha_1+\zeta_2))\frac{(\alpha_4+\zeta_1)}{\alpha_1\alpha_3\alpha_2\alpha_5} \\ N'_7 &= \zeta_2((\alpha_2-\zeta_1)(\alpha_4+\zeta_1))\frac{(\alpha_1+\zeta_2)}{\alpha_2\alpha_4\alpha_3\alpha_6} \\ N'_8 &= \zeta_1((\alpha_3-\zeta_2)(\alpha_1+\zeta_2))\frac{(-\alpha_2+\zeta_1)}{\alpha_1\alpha_3\alpha_4\alpha_5} \\ N'_9 &= ((\alpha_2-\zeta_1)(\alpha_4+\zeta_1))\frac{(\alpha_3-\zeta_2)(\alpha_1+\zeta_2)}{\alpha_2\alpha_4\alpha_1\alpha_3} \end{aligned} \tag{7}$$

with

$$\begin{aligned} \alpha_i &= 1-b_i \quad i=1,4 \\ \alpha_5 &= \alpha_2+\alpha_4 \\ \alpha_6 &= \alpha_1+\alpha_3 \end{aligned}$$

where for regular surface elements QQIE, not adjacent to the crack tip and the crack line, the parameters b_i are equal to zero (continuous 9-noded quadratic quadrilateral element). These specific parameters b_i are shown in Fig. 2b.

Asymptotic crack-tip fields in a creeping material

The material behavior in this paper is described by the elastic-nonlinear viscous constitutive relation according to the power law relation (Nortran, 1929)

$$\dot{\varepsilon} = \frac{\dot{\sigma}}{E} + \dot{\varepsilon}_0\left(\frac{\sigma}{\sigma_0}\right)^m \tag{8}$$

where E is the elasticity modulus, σ_0 is a reference stress, $\dot{\varepsilon}_0$ is a reference creep strain rate and m is the creep exponent. Under the assumption of multiaxial stress states, the extension of Eq. (8) can be read as

$$\begin{aligned}\dot{\varepsilon}_{ij} &= \dot{\varepsilon}^e_{ij} + \varepsilon^n_{ij}\\ \dot{\varepsilon}^e_{ij} &= \frac{1+\nu}{E}\dot{S}_{ij} + \frac{1-2\nu}{3E}\dot{\sigma}_{kk}\delta_{ij}\\ \dot{\varepsilon}^n_{ij} &= \frac{3}{2}\dot{\varepsilon}_0\left(\frac{\sigma_e}{\sigma_0}\right)^{m-1}\frac{S_{ij}}{\sigma_0}\end{aligned} \tag{9}$$

where S_{ij} are the components of the deviatoric stress tensor and $S_{ij} = \sigma_{ij} - \sigma_{kk}\delta_{ij}/3$ and σ_e is the Misses effective stress defined by $\sigma_e = \left((3/2)S_{ij}S_{ij}\right)^{1/2}$.

From the inspection of Eqs. (8) and (9) it could be noted that if there is a singular crack tip field at time $t = 0$ the elastic singularity fields prevail at the crack tip. In subsequent time step and at distances sufficient close to the crack tip the creep strain part of the total strain rate is much larger than the elastic strain rates and it seems to control the crack tip fields ($m > 1$). Thus, the constitutive equations (8) and (9) become power law creep relationships. Using the Hoff analogy (1954) to contrast the power-law creep relation with the power-law hardening relation, Riedel and Rice (1980) and Ohji et al. (1979) presented the HRR-type singularity fields for power-law creep material described by the equations

$$\begin{aligned}\sigma_{ij} &= \sigma_0\left(\frac{C(t)}{\dot{\varepsilon}_0\sigma_0 I_n r}\right)^{\frac{1}{n+1}}\tilde{\sigma}_{ij}(\theta)\\ \dot{\varepsilon}_{ij} &= \dot{\varepsilon}_0\left(\frac{C(t)}{\dot{\varepsilon}_0\sigma_0 I_n r}\right)^{\frac{n}{n+1}}\tilde{\varepsilon}_{ij}(\theta)\\ \dot{u}_i &= \dot{\varepsilon}_0 r\left(\frac{C(t)}{\dot{\varepsilon}_0\sigma_0 I_n r}\right)^{\frac{n}{n+1}}\tilde{u}_{ij}(\theta)\end{aligned} \tag{10}$$

where the radial distance r from the crack tip and the angle θ in relation to the x-axis are also shown in Fig. 1. The dimensionless constants I_n and the θ-variation functions of the suitably normalized functions $\tilde{\sigma}_{ij}, \tilde{\varepsilon}_{ij}$ and $\tilde{u}_{ij}$ depend on the creep exponent m and have been tabulated in Shih (1983).

The amplitude factor $C(t)$ of Eqs. (10) depends upon application time, magnitude of the remote loading, crack configuration and material properties. It is known from the finite element work of Bassani and McClintock (1981) that, on any closed path S surrounding a crack tip that lies within a region where the creep strain rates given by Eqs. (8) greatly exceed the elastic ones one can obtain the energy rate contour integral

$$C(t) = \int_S \left[\left(\frac{m}{m+1}\sigma_{ij}\dot{\varepsilon}_{ij} - \sigma_{11}\frac{\partial\dot{u}_1}{\partial x_1} - \sigma_{21}\frac{\partial\dot{u}_2}{\partial x_1}\right)\mathrm{d}x_2 + \left(\sigma_{12}\frac{\partial\dot{u}_1}{\partial x_1} + \sigma_{22}\frac{\partial\dot{u}_2}{\partial x_1}\right)\mathrm{d}x_1\right] \tag{11}$$

where S is a vanishingly small clockwise contour surrounding the crack tip and u_1, u_2, ε_{ij} and σ_{ij} are displacements, stresses and strains, respectively, evaluated along contour S. It is clear that $C(t)$ integral characterizes the intensity of the near tip fields in elastic-nonlinear viscous materials in precisely the same manner as the J-integral does the near tip fields in rate-independent elastic–plastic materials.

Analogous to the plastic analysis, a creep zone can also be defined by assuming the stress field outside the zone is essentially the same as elastic stress field and its size can be estimated as

$$r_c(\theta, t) = \beta_c(m,\theta)\left(\frac{K^2}{2\pi}\right)^{\frac{m+1}{m-1}}\left[\frac{I_n}{BC(t)}\right]^{\frac{2}{m-1}} \tag{12}$$

where r_c is the creep zone size, K is the known elastic stress concentration factor and $\beta_c(m,\theta)$ a non-dimensional angular function. The factor I_n is accounting for stress states while the constant $B = \dot{\varepsilon}_0/\sigma_0^m$.

In the long time term, as the creep zone grows an extensive creep condition is achieved and the path and time dependent energy rate contour integral approaches a constant value C^*. It has been shown that over the entire transition regime $C(t)$ can be approximated by the empirical formula

$$C(t) \cong C^*\left(1 + \frac{t_T}{t}\right) \tag{13}$$

where t_T is the transition time from small scale creep to extensive creep which is given by

$$t_T = \frac{(1-\nu^2)K^2}{(m+1)EC^*} \tag{14}$$

Special singular boundary element implementation

To produce a special element which presents the above mentioned HRR-type singularity of Eqs. (10) at the crack tip (Fig. 1), the standard quadratic shape function for displacement rates should be manipulated. Thus, by modifying properly (Maiti, 1992) the displacement rate standard quadratic shape functions of (5), one can obtain the following new set of shape functions N^u_a which depend upon the creep exponent m

$$\begin{aligned}N^u_1 &= 2^{\frac{1}{1+m}}\left[\left(\frac{r}{l}\right)^{1+\frac{1}{1+m}} - \left(\frac{r}{l}\right)^{\frac{1}{1+m}}\right] + \left(\frac{r}{l}\right)\\ N^u_2 &= 2^{1+\frac{1}{1+m}}\left[\left(\frac{r}{l}\right)^{\frac{1}{1+m}} - \left(\frac{r}{l}\right)^{1+\frac{1}{1+m}}\right]\\ N^u_3 &= 2^{\frac{1}{1+m}}\left[\left(\frac{r}{l}\right)^{1+\frac{1}{1+m}} - \left(\frac{r}{l}\right)^{\frac{1}{1+m}}\right] - \left(\frac{r}{l}\right) + 1\end{aligned} \tag{15}$$

where l is the length of the new special quadratic element, the distance $r = l - x$ and the ratio can be defined in terms of the intrinsic coordinate ζ as $(r/l) = (1-\zeta)/2$. Then, by taking the derivatives of the new shape functions (15) one can obtain the following

$$\frac{\partial N^u_1}{\partial x} = -\left(\frac{1}{l}\right) + 2^{\frac{1}{1+m}}\left(\frac{1}{1+m}\right)\left(\frac{1}{l}\right)\left(\frac{l-x}{l}\right)^{-\frac{m}{1+m}} - 2^{\frac{1}{1+m}+1}\left(\frac{1}{1+m}+1\right)\left(\frac{1}{l}\right)\left(\frac{l-x}{l}\right)^{\frac{1}{1+m}}$$

$$\frac{\partial N_2^u}{\partial x} = -2^{\frac{1}{1+m}+1}\left(\frac{1}{1+m}\right)\left(\frac{1}{l}\right)\left(\frac{l-x}{l}\right)^{-\frac{m}{1+m}} + 2^{\frac{1}{1+m}+1}\left(\frac{1}{1+m}+1\right)\left(\frac{1}{l}\right)\left(\frac{l-x}{l}\right)^{\frac{1}{1+m}}$$
$$\frac{\partial N_3^u}{\partial x} = \left(\frac{1}{l}\right) - 2^{\frac{1}{1+m}}\left(\frac{1}{1+m}\right)\left(\frac{1}{l}\right)\left(\frac{l-x}{l}\right)^{-\frac{m}{1+m}} - 2^{\frac{1}{1+m}+1}\left(\frac{1}{1+m}+1\right)\left(\frac{1}{l}\right)\left(\frac{l-x}{l}\right)^{\frac{1}{1+m}} \quad (16)$$

Now, it may be noted that the derivatives (16) display a $r^{-m/(m+1)}$ singularity near the crack tip which is the actual situation for the strain rate singularities according to (10). It may also be easily proved as in Maiti (1992) that the new set of displacement rate shape functions (15) fulfill the convergence criteria of the rigid body mode and the constant strain condition.

Since in boundary element methodology displacement and tractions are independently represented, the above derived singular element for the simulation of crack tip behavior of displacement rates, fails to model the expected from Eqs. (10) crack tip behavior of tractions which displays an order of $-1/(m+1)$ singularity. Thus, for the proper simulation of the traction rate singularity, different shape functions are derived by the use of the derivatives of the shape functions (16) and finally modified to the following separate forms N_a^t in terms of creep exponent m

$$N_1^t = 2^{\frac{m}{1+m}}\left[\left(\frac{l}{r}\right)^{\frac{1}{1+m}} - \left(\frac{r}{l}\right)^{\frac{m}{1+m}}\right] - 2 + 2\left(\frac{r}{l}\right)$$
$$N_2^t = 2^{\frac{m}{1+m}}\left[\left(\frac{l}{r}\right)^{\frac{1}{1+m}} - \left(\frac{r}{l}\right)^{\frac{m}{1+m}}\right] \quad (17)$$
$$N_3^t = 2^{\frac{m}{1+m}}\left[-\left(\frac{l}{r}\right)^{\frac{1}{1+m}} + \left(\frac{r}{l}\right)^{\frac{m}{1+m}}\right] + 1$$

where now $r = x$ and the ratio $(r/l) = (1+\zeta)/2$.

It is obvious, that the traction rate shape functions (17) have the proper order of traction rate singularity since have the dependence of $r^{-1/(m+1)}$ according to (10). It may also be noted from a proper derivation of (17) that the crack tip values of traction rate shape functions are given as expected by the following limiting processes

$$N_1^t = \lim_{r\to 0}\left(\frac{l}{r}\right)^{\frac{1}{1+m}},\quad N_2^t = \lim_{r\to 0}\left(\frac{l}{r}\right)^{\frac{1}{1+m}},\quad N_3^t = \lim_{r\to 0}\left(\frac{l}{r}\right)^{\frac{1}{1+m}} \quad \text{as } \frac{r}{l} = 0$$
$$N_1^t = 0,\quad N_2^t = 1,\quad N_3^t = 0 \quad \text{as } \frac{r}{l} = 0.5$$
$$N_1^t = 0,\quad N_2^t = 0,\quad N_3^t = 1 \quad \text{as } \frac{r}{l} = 1$$

A simultaneous simulation of displacement and traction rate fields, by the use of the shape functions (15) and (17), respectively, yields to the proposed, in the present BEM approach, creep strain-traction singular element (CR-STSE).

Interior surface elements adjacent to the crack tip

The modeling of the inelastic strain rate around the crack tip (Fig. 1) is performed here by means of semi-discontinuous 9-noded quadratic quadrilateral surface elements (QQIE) generated by the use of the interpolation functions (7) by just setting the appropriate values in parameters α_i. In this case two different meshes should be defined: the geometric mesh which is defined by the nodes which lie on the boundary of the surface elements and the functional mesh (Fig. 2b) which is defined by the functional nodes which lie within the element boundaries in such a way that any functional node does not coincide with the crack tip geometric node.

4 Matrix formulation

The isoparametric boundary element representation of the integral equations (2) and (3) utilizing the function expansions (5), (7), (15) and (17) can be written as

$$(\delta_{ij} - C_{ij})\dot{U}_j(\xi) = \sum_{l=1}^{L}\left(\int_{\Gamma_l} N_a(\zeta)U_{ij}^*(\xi,\tilde{X}(\zeta))\mathrm{d}\Gamma(\tilde{X})\right)\dot{P}_j^a - \sum_{l=1}^{L}\left(\int_{\Gamma_l} N_a(\zeta)T_{ij}^*(\xi,\tilde{X}(\zeta))\mathrm{d}\Gamma(\tilde{X})\right)\dot{U}_j^a + \sum_{n=1}^{N}\left(\int_{\Omega_n} N_b'(\zeta_1,\zeta_2)\Sigma_{jki}^*(\xi,\tilde{x}(\zeta_1,\zeta_2))\mathrm{d}\Omega(\tilde{x})\right)\dot{E}_{jk}^{n^b} + \alpha\sum_{n=1}^{N}\left(\int_{\Omega_n} N_b'(\zeta_1,\zeta_2)\bar{\Sigma}_{jki}^*(\xi,\tilde{x}(\zeta_1,\zeta_2))\mathrm{d}\Omega(\tilde{x})\right)\dot{T}^b \quad (18)$$

and

$$\dot{\sigma}_j(\xi) = \sum_{l=1}^{L}\left(\int_{\Gamma_l} N_a(\zeta)\bar{U}_{ij}^*(\xi,\tilde{X}(\zeta))\mathrm{d}\Gamma(\tilde{X})\right)\dot{P}_j^a - \sum_{l=1}^{L}\left(\int_{\Gamma_l} N_a(\zeta)\bar{T}_{ij}^*(\xi,\tilde{X}(\zeta))\mathrm{d}\Gamma(\tilde{X})\right)\dot{U}_j^a + \sum_{n=1}^{N}\left(\int_{\Omega_n} N_b'(\zeta_1,\zeta_2)\tilde{\Sigma}_{jki}^*(\xi,\tilde{x}(\zeta_1,\zeta_2))\mathrm{d}\Omega(\tilde{x})\right)\dot{E}_{jk}^{n^b} + \alpha\sum_{n=1}^{N}\left(\int_{\Omega_n} N_b'(\zeta_1,\zeta_2)\tilde{\bar{\Sigma}}_{jki}^*(\xi,\tilde{x}(\zeta_1,\zeta_2))\mathrm{d}\Omega(\tilde{x})\right)\dot{T}^b \quad (19)$$

with L being the number of boundary elements and N the number of interior surface elements; Γ_l is the lth boundary

elements ($\Gamma = \sum \Gamma_l$) and Ω_n is the nth surface element ($\Omega = \sum \Omega_n$); $U^*_{ij}, T^*_{ij}, \Sigma^*_{jki}$ and $\bar{\Sigma}^*_{jki}$ and $\bar{U}^*_{ij}, \bar{T}^*_{ij}, \bar{\Sigma}^*_{jki}$ and $\bar{\bar{\Sigma}}^*_{jki}$ are the corresponding tensors for the boundary integrals and inelastic and thermal effect tensors for surface integrals of Eqs. (18) and (19), respectively. The evaluation of the coefficients of the matrices in these equations needs a number of complicated integration procedures. Since analytical integration of the integrals in these equations is not possible in general, the Gaussian quadrature technique was used. For the singular cases which occur when the field and the source point are situated over the same element, special approaches were employed as in the work of Providakis (1996). The evaluation of the singular surface inelastic and temperature rates profile integrals was done by subdividing each 9-noded quadratic quadrilateral interior element into a number of triangular subelements with their appexes located at the origin point.

Then, by applying a boundary nodal point collocation procedure to Eqs. (18) and (19) one can obtain the following system of equations in matrix form

$$[A]\{\dot{u}\} = [B]\{\dot{\tau}\} + [E]\{\dot{\varepsilon}^n\} + [T]\{\dot{b}^T\} \tag{20}$$

$$\{\dot{\sigma}\} = [\tilde{B}]\{\dot{\tau}\} + [\tilde{E}]\{\dot{\varepsilon}_n\} + [\tilde{T}]\{\dot{b}^T\} \tag{21}$$

where the coefficients of matrices $[A]$ and $[B]$ contain integrals with variables of the type

$$\int_{\Delta\Gamma_q} T^*_{ij}(\xi, \tilde{\boldsymbol{x}}(\zeta))\mathrm{d}\Gamma_q, \qquad \int_{\Delta\Gamma_q} U^*_{ij}(\xi, \tilde{\boldsymbol{x}}(\zeta))\mathrm{d}\Gamma_q \tag{22}$$

and the matrices $[E]$, $[\tilde{E}]$ and $[\tilde{T}]$ and $[T]$, involve X^*_{jki} and $\bar{X}^*_{jki}$ integral terms, respectively. However, the vector $\{\dot{\varepsilon}^n\}$ is known at any time through the constitutive equations (9) and the stress rates of Eq. (21) while the vector $\{\dot{b}^T\}$ through the assumed solution of the appropriate steady state diffusion equation subject to slowly varying surface temperatures. Half of the total number of components of $\{\dot{u}\}$ and $\{\dot{\tau}\}$ are prescribed through the boundary condition while the other half are unknowns.

Time integration algorithm

The initial distribution of the state variables have to be prescribed while the initial value of the nonelastic strain is set to zero. Thus, the only existed strains at time step $t = 0$ are elastic and then, the thermal and initial stresses and displacements can be obtained from the solution of the corresponding elastic problem. By the use of Eqs. (20) and (21) the displacement and stress rates can be obtained at time step $t = 0$ while the rates of change of the state variables can be computed from constitutive equations. Thus, the initial rates of all the relevant variables are now known and their values at a new time Δt can be obtained by integrating forward in time. The rates are then obtained at time Δt and so on, and finally the time histories of all the variables can be computed. Another important task in this approach is the choice of a suitable time integration scheme. For the purposes of the present paper, an Euler type algorithm with automatic time-step control is employed. The automatic time-step control procedure is based on comparison of a suitable defined error e with prescribed error limits $e_{\min}$ and $e_{\max}$. The initial time-step must be also prescribed. The m-th time step at time Δt_m can be derived on the basis of its estimate $E\Delta t_m$ in terms of the single differential equation

$$\frac{\mathrm{d}y}{\mathrm{d}t} = F(y, t) \tag{23}$$

Then the algorithm can be proceeded as follows

if $e_{\max} < e$: replace estimates $E\Delta t_m$ by $E\Delta t_m/2$ and then recompute e
if $e_{\min} < e < e_{\max}$: compute estimate $E\Delta t_{m+1} = \Delta t_m$
if $e \le e_{\min}$: compute estimate $E\Delta t_{m+1} = 2\Delta t_m$

The energy rate contour integral $C(t)$ is then evaluated numerically as a function of time through the computed values of stress, strain and displacement rates from the above mention algorithm and the use of integral equation (11) for different paths. Each path is decomposed into sufficient number of straight segments and the integral over each segment is obtained by Gaussian quadrature (ten Gauss points).

5 Numerical results

Example 1

To validate the proposed approach a shallow-edge cracked semicircular plate in plane strain deformation is considered. A similar example is also presented in the finite element work of Bassani and McClintock (1981). This semicircular plate is assumed to be subjected to a suddenly applied Mode I remote tensile loading of a uniformly distributed magnitude of value $\sigma_N = \sigma_0 = E/2000$. The plate has a radius equal to $21a$ where a is the crack length. All results are for Poisson ratio $v = 0.3$ and creep exponent $m = 3$. A typical interior mesh for this example is shown in Fig. 3a, b. The creep stress relaxation is plotted in Fig. 4 as obtained by the present boundary element methodology in association with the use of the CR-STSE simulations and the FEM methodology of Bassani and McClintock (1981). The agreement is good especially for time $t > t_N$ where time $t_N = (\sigma_N/E)/\dot{\varepsilon}_0(\sigma_N/\sigma_0)^m$. The differences which are existed between the two solutions in short time are coming, probably, from some errors arising in the solution of Bassani and McClintock (1981) due to the use of crack tip finite elements which exhibit strain singularity of r^{-1} which do not effectively approximate the actual strain singularity of $r^{-m/(m+1)}$. The steady state value of the ratio $\sigma_{e_{\max}}/\sigma_N$ of the maximum effective stress ($\sigma_e = (\frac{3}{2}S_{ij}S_{ij})^{3/2}$) to the applied stress σ_N is equal to 4.2 in contrast to the value 4.28 of Bassani and McClintock (1981).

Example 2

Consider a typical single edge notched tension specimen (SENT) under mode I plane strain conditions. The specimen has a shallow edge crack of a depth given by $a/w = 0.125$ and width $w = 101.6$ cm. The material of the specimen is described by the power law creep relations (8) and have the values: $E = 153.717$ GPa, $\sigma_0 = 417.057$ MPa, $v = 0.33$, $m = 5$ and the constant $B = 2.1 \times 10^{-27} \times (6.895 \times 10^{-3}\,\text{MPa})^{-5}$/h. The specimen is assumed to be subjected to a remote uniform load of 206.85 MPa which is applied instantaneously and then hold constant until steady-state creep conditions are reached. Initial application of the load is assumed to occur so quickly that it involves purely elastic response. Due to the symmetry of the specimen a half of the specimen was modeled (Fig. 5a, b).

As it is stated above the creep zone boundary is defined as the region where the effective creep strain ε_e^c equals the effective elastic strain ε_e^e, with $(\varepsilon_e = ((2/3)\varepsilon_{ij}\varepsilon_{ij})^{1/2})$. Thus, by taking the locus of the interior points which satisfy this equality, the shape of the creep zone for the specimen under investigation can be shown in Fig. 6 for time steps $t = 0.1t_T$, $t = t_T$ and $t = 2_T$ with transmission time t_T equal to 225 h as obtained by using Eq. (14) and the value of $C^* = 0.797$ MPa-cm/h yielded from the equations (Li et al. 1988)

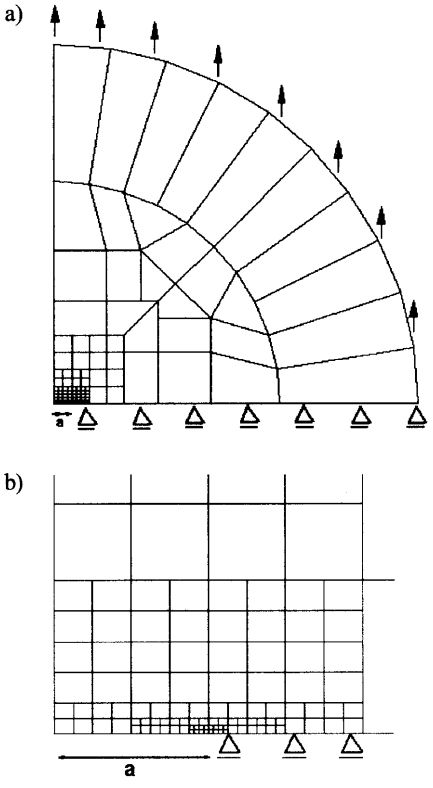

Fig. 3. **a** Interior mesh for the semi-circular plate in plane strain. **b** Further details of the interior mesh at the vicinity of the crack-tip

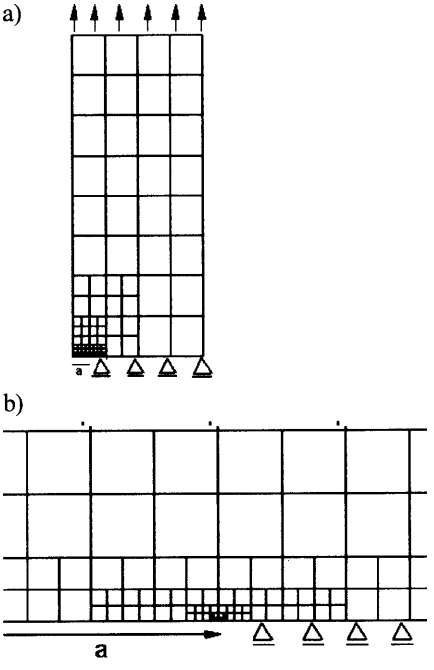

Fig. 5. **a** Interior mesh for the typical SENT specimen. **b** Further details of the interior mesh at the vicinity of the crack-tip

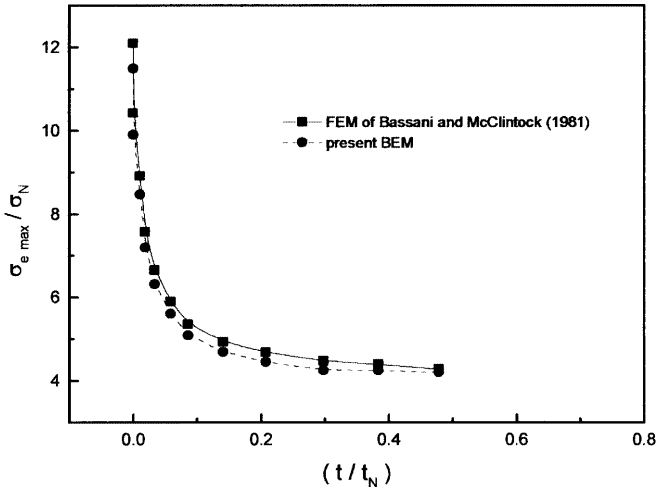

Fig. 4. Creep stress redistribution as a function of time

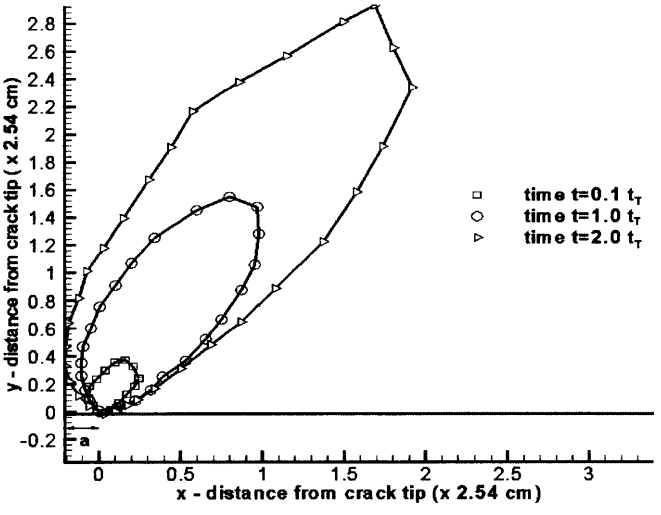

Fig. 6. Creep zone growth in SENT specimen

$$C^* = B(w-a)(a/w)h_1(a/w,n)(P\sigma_0/P_0)^{\tilde{n}+1}$$
$$P_0 = 1.455\tilde{n}(w-a)\sigma_0 \qquad (24)$$
$$\tilde{n} = \left(1+\left(\frac{a}{w-a}\right)^2\right)^{1/2} - \left(\frac{a}{w-a}\right)$$

where P is the applied load and h is a dimensionless function given in terms of the creep exponent m and the ratio a/w and is tabulated in Kumar et al. (1981).

The depicted in Fig. 6 creep zone agrees well in shape with those presented in Ehlers and Riedel (1981). It can be also observed that the creep strain dominates inside creep zone, while, as expected, the elastic strain prevails outside the creep zone.

The time dependence of the energy rate contour integral $C(t)$ is numerically evaluated by integration of Eq. (11) along a path with radial distance $r = 0.018a$ from the crack tip and shown in Fig. 7. It is found that for long time $(t > 0.35t_T)$ the contour integral $C(t)$ as obtained by the present BEM approach is in agreement with that obtained by using the approximation formula (13) in association with the values $C^* = 0.797$ MPa-cm/h and $t_T = 225$ h. It is also observed from Fig. 7 that at time about $t = 3.5t_T$ the integral $C(t)$ approaches the steady state value $C^* = 0.797$ MPa-cm/h as calculated from equations (Li et al., 1988).

The creep stress relaxation for the SENT specimen at time $t = 0.1t_T$ along the crack line is depicted in Fig. 8 as obtained by the use of the present BEM and the finite element methodology of commercial FEM software MSC.Marc (2000). The MSC.Marc mesh was comprised of 150 8-node isoparametric finite elements. The solution between the two methods compares well.

Example 3

Consider a typical compact tension (CT) fracture test specimen with width $w = 26$ mm and thickness $B_h = 13$ mm. The specimen contains a crack of length $a = 13$ mm and is assumed to be subjected to a external load of $P = 7$ kN. The material properties are $E = 181$ GPa, $v = 0.34$, $B = 2.65 \times 10^{-56}$ (MPa^{-m})/h and creep exponent $m = 18.27$. The load of $P = 7$ kN is assumed to be applied to a rigid pin constructed to fit the hole as shown in the mesh depicted in Fig. 9a, b. The normalized values of energy rate contour integral $C(t)$ are shown in Fig. 10. The path dependence of the $C(t)$ integral is proved by its evaluation in different paths (r/a) as presented in Fig. 10. The accuracy of the present BEM approach is verified by the good agreement of the present results using Eq. (11) and the results obtained from the formula (13). Here, the fully plastic J-integral values for power law hardening plasticity (Kumar et al., 1981) can be directly used as the C^* values for power law creep of the CT specimen. A comparison of the steady-state value C^* as computed by the present BEM approach and that derived from the fully plastic J-integral results is shown in Fig. 11 as a function of the applied load P. A very good agreement is obtained which again confirms the validity of the proposed BEM in association with the use of the proposed CR-STSE boundary element.

6 Conclusions

In this paper a new boundary element approach which is based on the implementation of a special singular boundary element is presented for the evaluation of the

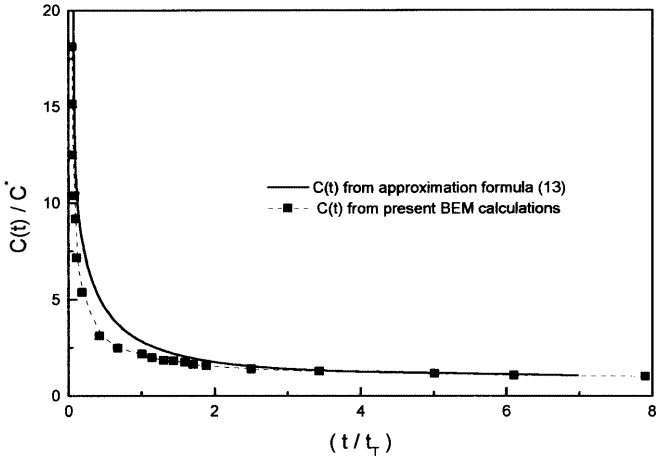

Fig. 7. Time dependence of integral $C(t)$

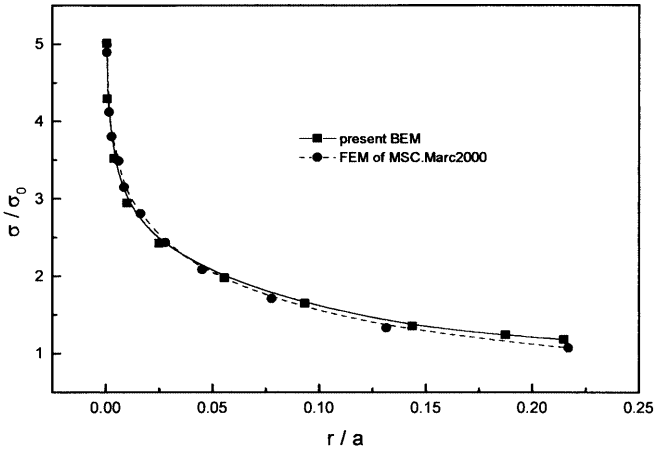

Fig. 8. Creep relaxation in SENT specimen at $t = 0.1t_T$

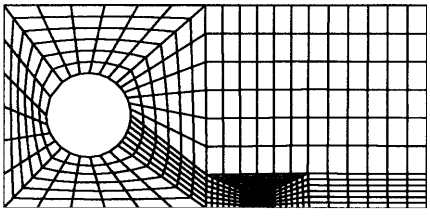

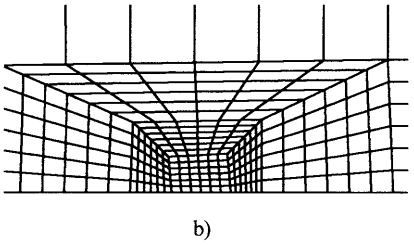

Fig. 9. a Interior mesh for the typical CT specimen. **b** Further details of the interior mesh at the vicinity of the crack-tip

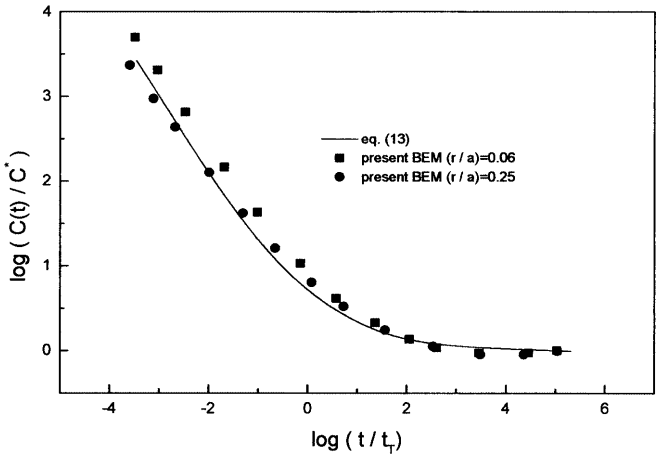

Fig. 10. Energy contour integral $C(t)$ as a function of time for CT specimen

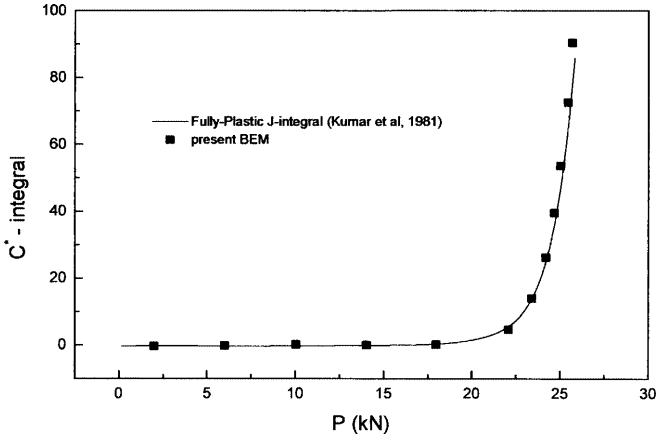

Fig. 11. Energy contour integral $C(t)$ as a function of applied load P for CT specime

crack tip fields arising in creeping structural components plates under the effect of remote loading condition. The new singular element is easy to implement and do not pose any problem in the resulted system of integral equation or in solving them. This new BEM approach yields comparable in accuracy results with those obtained by finite element methodologies and available empirical solutions for this kind of time dependent fracture analysis problems.

The present results cannot be considered as conclusive, since the proposed CR-STSE singular boundary element approach needs to be applied to more complex creep fracture problems containing unsymmetric or interacting crack patterns which are immediate follow up steps for this kind of BEM analysis.

References

Aliabadi MH (1997) Boundary element formulations in fracture mechanics. Appl. Mech. Rev. 50(2): 83–96

Bassani JL, McClintock FA (1981) Creep relaxation of stress around a crack tip. Int. J. Solids Struct. 17: 479–492

Beskos DE (1987) Numerical methods in dynamic fracture mechanics. EUR-11300 EN, Joint Research Center of EC Ispra Establishment, Ispra, Italy

Blandford GE, Ingraffea AR, Ligget JA (1981) Two dimensional stress intensity factor computations using the boundary element method. Int. J. Num. Meth. Eng. 17: 387–404

Cruse TA, Polch EZ (1986) Application of an elstoplastic boundary element method to some fracture mechanics problems. Eng. Fract. Mech. 23: 1085–1096

Ehlers R, Riedel H (1981) A finite element analysis of creep deformation in a specimen containing a macroscopic crack. In: Proceedings of the Fifth International Conference on Fracture, Pergamon Press, Oxford, pp. 691–698

Hantschel T, Busch M, Kuna M, Maschke HG (1990) Solution of elastic–plastic crack problems by an advanced boundary element method. In: Luxmoore AR, Owen DRJ (eds), Numerical Methods in Fracture Mechanics, Pineridge Press, Swansea, pp. 29–40

Hoff NJ (1954) Quarterly Appl. Mech. 12: 49–55

Hutchinson JW (1968) Singular behavior at the end of a tensile crack in a hardening material. J. Mech. Phys. Solids 16: 13–31

Kumar V, German MD, Shih CF (1981) An engineering approach to elastic–plastic analysis. EPRI NP-1931, Electric Power Research Institute, Palo Alto, CA

Leitao V, Aliabadi MH, Rooke DP (1995) The dual boundary element formulation for elastoplastic fracture mechanics. Int. J. Num. Meth. Eng. 38: 315–333

Li FZ, Needlemen A, Shih CF (1988) Characterization of near tip stress and deformation fields in creeping solids. Int. J. Fract. 36: 163–186

Maiti SK (1992) A finite element for variable order singularities based on the displacemenet formulation. Int. J. Num. Meth. Eng. 33: 1955–1974

Morjaria M, Mukherjee S (1981) Numerical analysis of planar, time-dependent inelastic deformation of plates with cracks by the boundary element method. Int. J. Solids Struct. 17: 127–143

Morjaria M, Mukherjee S (1982) Numerical solution of stresses near crack tips in time-dependent inelastic fracture mechanics. Int. J. Fract. 18(4): 293–310

MSC.Marc (2000) MSC.Software Corporation, Los Angeles, CA

Mukherjee S (1977) Corrected boundary integral equations in planar thermoelastoplasticity. Int. J. Solids Struct. 13: 331–335

Nortran FH (1929) The Creep of Steel at High Temperatures. McGraw-Hill, New York

Ohji K, Ogura K, Kubo S (1979) Stress-strain field and modified J-integral in the vicinity of crack tip under transient creep conditions. Japanese Soc. Mech. Eng. 790(13): 18–20

Providakis CP (1996) A general and advanced boundary element transient analysis of elastoplastic plates. Eng. Anal. Bound. Elem. 17: 133–143

Rice JR, Rosengren GF (1968) Plane strain deformation near a crack tip in a power-law hardening material. J. Mech Phys. Solids 16: 1–12

Riedel H (1978) Zeitschrift fur Metallkunde 69(12): 755–760

Riedel H (1979) Creep deformation at crack-tips in elastic-viscoplastic solids. MRL E-114 Technical Report, Materials Research Laboratory, Brown University, RI

Riedel H, Rice JR (1980) Tensile cracks in creeping solids. Fracture Mechanics: Twelfth Conference, ASTM STP 700: 112–130

Rußwurm S (1992) Berechung elastoplastischer Rißprobleme mittels der Randelementmethode, Fortschr-Ber VDI, Reihe 18 Nr 104, VDI Verlag

Shih CF (1983) Tables of Hutchinson-Rice-Rosengren singular field quantities. MRL E-147, Division of Engineering, Brown University, RI

Tan CL, Lee KH (1983) Elastic–plastic stress analysis of a cracked thin-walled cylinder. J. Strain Anal. 50–57